Underpotential and Electroless Pb Monolayer Deposition on Ru(0001)

D. Wu,[1] K. Ahmadi,[2,*] N. Dole,[3,] A. Joi,[3] Y. Dordi,[3] and S. R. Brankovic[1,2,**,z]**

[1]*Electrical and Computer Engineering Department, University of Houston, Houston, Texas, USA*
[2]*Material Science Program, University of Houston, Houston, Texas, USA*
[3]*Lam Research Corporation, Fremont, California, USA*

The work reporting a detailed and comparative study of Pb UPD and Pb e-less ML deposition on Ru(0001) substrate is presented. The electrochemical results are analyzed through the scope of the adsorption isotherm formalism where parameters describing the thermodynamics of deposited Pb monolayer obtained by each process are compared. In addition to these results, the in situ STM and electrochemical quartz micro balance data are presented for each process identifying the mutual mechanistic similarities and differences between electroless Pb and underpotential Pb monolayer. Considerable applications of Ru metal in microelectronics and catalysis rise significance of these results for variety of future developments in these areas.
 [DOI: 10.1149/2.0101910jes]

Manuscript received April 12, 2019. Published May 24, 2019.

The underpotential deposition (UPD) has been widely studied phenomenon since the early days.[1–4] It involves formation of a two-dimensional (2D) monolayer (ML) of one metal onto foreign substrate preceding its bulk deposition. This fact is used to design diverse electrodeposition protocols where UPD ML act as surfactant or flux mediator improving the growth kinetics and deposit morphology.[5,6] UPD MLs are also used in catalysis[7] and in surface characterization studies.[8–11] More recent applications include ML restricted deposition methods where UPD phenomenon serves as enabling process.[12–16] Along these efforts, a very exciting development has been demonstrated with the first reports of an electroless (e-less) Pb and Zn ML deposition phenomenon.[17–20] Detailed analysis of these results suggest that e-lessly deposited Pb ML has a UPD-like properties[18,19] and thus pertains to a wide variety of applications already demonstrated for its UPD counterpart. Moreover, the e-less ML deposition represents a surface selective and self-terminating process which facilitates development of two-step e-less atomic layer deposition (e-less ALD) protocol.[18–20]

In general, the UPD can be phenomenologically described as potential dependent adsorption.[1] The characteristic cyclic voltammetry (CV) involves one or more deposition/stripping peaks in the underpotential region of particular metal. The complexity of voltammetry arises from existence of one or more UPD ML superstructures[21,22] and/or one or more UPD MLs formed.[23,24] The adsorption behavior of UPD ML is mainly determined by the interactions between the UPD metal and the substrate, and interactions between adatoms within the UPD ML.[25–28] Other effects such as strain and anion co-adsorption were found important as well. In the quest for proper description of UPD one usually resorts to analytical expression which describes the underpotential vs. coverage relation i.e. the UPD isotherm. *Burkenstain-Shwatterian* (S&B) isotherm is a commonly used one and can be applied to wide variety of systems. If UPD is a single phase system, it is formulated as follows:[29]

$$\Delta E = \Delta E_{\theta\to 0} - \frac{RT}{m\cdot F}\cdot\left[\ln\left(\frac{\theta}{1-\theta}\right) + f\theta + g\theta^{3/2}\right] \qquad [1]$$

Here m represents the electrosorption valence of the UPD metal ion, and $\Delta E_{\theta\to 0}$ term represents the underpotential of the most positive stripping/deposition peak where UPD ML coverage approaches zero. The f and g terms are *Temkin* and *Frumkin* parameters describing the UPD ML-substrate and UPD adatom-adatom interaction. Terms F and R are fundamental constants while T stands for absolute temperature. The same isotherm formulation is found also applicable in demonstrating the adsorption behavior of e-lessly deposited Pb ML. If combined with rate equation of the overall redox process, it yields the expression which successfully models the open circuit potential (OCP) transients obtained during the e-less Pb ML deposition:[19]

$$\begin{aligned} E = \Delta E_{\theta\to 0} - \frac{RT}{mF} \\ \cdot\left\{\ln\left(\frac{(\Delta r_S/(\Delta r_{ML}-\Delta r_S))\cdot\left(\exp(t/(\Delta r_{ML}-\Delta r_S))-1\right)}{1-(\Delta r_S/(\Delta r_{ML}-\Delta r_S))\cdot\left(\exp(t/(\Delta r_{ML}-\Delta r_S))-1\right)}\right)\right. \\ + f\cdot(\Delta r_S/(\Delta r_{ML}-\Delta r_S))\cdot\left(\exp(t/(\Delta r_{ML}-\Delta r_S))-1\right) \\ \left. + g\cdot\left((\Delta r_S/(\Delta r_{ML}-\Delta r_S))\cdot\left(\exp(t/(\Delta r_{ML}-\Delta r_S))-1\right)\right)^{3/2}\right\}. \end{aligned} \qquad [2]$$

In the above expression, the net production rates of electrons for Pb^{2+} ion reduction are recognized separately for the clean substrate surface (Δr_S) and for the substrate surface covered by Pb ML (Δr_{ML}).

In this paper we report a detailed and comparative study of Pb UPD and Pb e-less ML deposition on Ru(0001) substrate. The electrochemical results are analyzed through the scope of the adsorption isotherm formalism where parameters describing thermodynamics of deposited Pb ML obtained by each process are compared. In addition to these results, the in situ STM and ECQMB data are presented for each process identifying the mutual mechanistic similarities and differences during the nucleation and growth stage. Considerable applications of Ru metal in microelectronics[14] and catalysis[30,31] increase the significance of these results for variety of future developments in these areas. Some of them may include development of new Pb ML aided thin film growth protocols or new catalyst ML synthesis routes on Ru substrate.

Experimental

General details.—The starting Ru(0001) was disk with diameter of 10 mm and 2 mm thickness, (Monocrystals Company). It was prepared using mechanical polishing and induction annealing in 75% H_2 + 24% N_2 + 1% CO gas mixture at 1400°C for 60 min. This routinely yielded a highly reflective mirror-like surface with very reproducible Pb UPD voltammetry (Figure 1). All solutions for Pb UPD and Pb e-less ML deposition were prepared with high purity grade chemicals (99.999%, Alfa Aaeser, Merck) and >18.2 MΩ ultra-pure water (Millipore Direct Q-UV with Barnstead A1007 pre-distillation unit). Before each experiment, solutions were de-aerated for one hour with ultrapure nitrogen in order to minimize concentration of dissolved oxygen from air. All experiments are performed using ultraclean glassware and oxygen-free environment. The volume of the electrochemical

*Electrochemical Society Student Member.
**Electrochemical Society Member.
ᶻE-mail: SRBrankovic@uh.edu

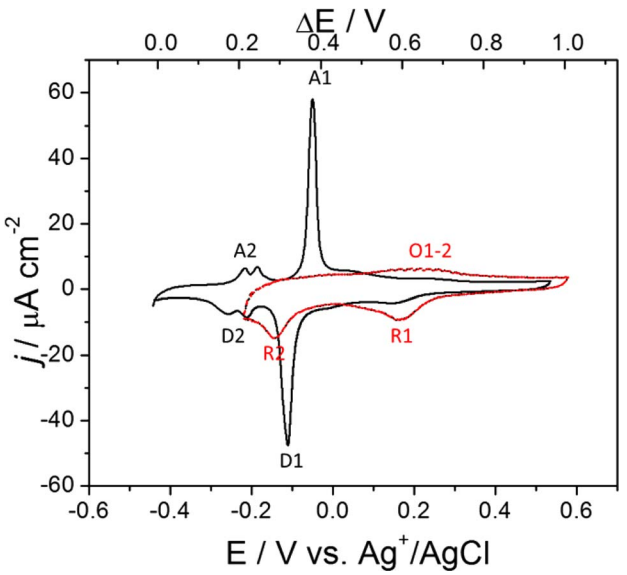

Figure 1. The CV for Pb UPD process in 0.1M HClO4+10^{-3} M Pb^{2+} solution (black) and Ru surface in 0.1 M $HClO_4$ (red). Sweep rate: 0.05 V·s^{-1}.

cell was 0.150 dm^3 while the solution volume was standardized to 0.1 dm^3 for each experiment. The solution volume during electrochemical quartz microbalance (ECQMB) and in situ scanning tunneling microscopy (STM) studies was 0.001 dm^3. The quartz microbalance sample was a 5 nm Ru layer deposited on 50 nm thick gold film on quartz crystal with resonant frequency of ≈ 6 kHz. The hanging meniscus electrode configuration was used for all electrochemical studies. Potentials in the text and figures are presented either as the value of Pb-underpotential, ΔE or as a potential (E) vs. silver-silver chloride reference electrode (Ag/AgCl/1.0 M KCl; $E = 0.235$ V vs. SHE). The electrochemical studies were performed using BASi Epsilon system, while STM images were recorded using Nanoscope V controller with multimode scanner unit (Veeco instruments). The STM tips were made of PtIr wire coated with apiezon wax to minimize faradic current contribution to the tunneling signal. The solution for e-less Pb ML deposition was prepared by mixing two volume parts of solution containing Pb^{2+} ions ($Pb(ClO_4)_2$) and one volume part of the solution containing V^{2+} ions as reducing agent (VCl_2). Both solutions contained 0.1 M $HClO_4$ as a background electrolyte. The nominal concentrations of Pb^{2+} and V^{2+} in solution for e-less Pb ML deposition are presented in Table I.

Experimental routine for e-less Pb ML deposition.—All deposition experiments and OCP measurements during the e-less Pb ML deposition were performed in N_2 filled glove box. Each experiment involved three steps. They are briefly explained below:

1) Step one: First, the cyclic voltammetry measurements were performed to verify the quality of the surface and characteristics of the Pb UPD process on a Ru(0001).
2) Step two: The potential control is switched off and the OCP transients are recorded during addition of V^{2+} containing aliquot. Typical length of the OCP measurements was between 50–200 seconds.
3) Step three: Sample with deposited e-less Pb ML is transferred to a well de-aerated 0.1 M $HClO_4$ solution where linear sweep is performed in anodic direction to strip the Pb ML and record the stripping wave.

Table I. Solutions for the e-less Pb ML deposition.

	e-less Pb ML Dep.
	0.1 M $HClO_4$
	0.001/0.00066 M Pb^{2+}
	0.003 M V^{2+}
	0.0003 M Cl^-

The same experimental routine is performed during ECQMB measurements, except the third step which was omitted.

STM image processing.—The STM images of the Pb UPD process on Ru(0001) were analyzed using custom made digital image processing (DIP) algorithm.[32] For this purpose, a threshold value to segment each image into a binary image has been determined using an autonomous global thresholding method.[33] The image segmentation was used for differentiation and identification of each nanocluster on the surface. This analysis provided an objective information about the number of Pb nanoclusters on Ru(0001) terraces, the mean/representative size of the nanoclusters, their coverage and height.[34]

Results and Discussion

Pb UPD on Ru(0001).—Representative cyclic voltammetry (CV) of the Pb UPD process on Ru(0001) surface from 0.1M $HClO_4 + 10^{-3}$ M Pb^{2+} solution is shown in Figure 1 – black line. A closer investigation of the cathodic scan shows two distinct deposition peaks, D1 and D2, occurring at approximately 0.32 V and 0.2 V underpotentials (ΔE). The latter one is very sensitive to the scan rate and it completely disappears from the voltammogram if the scan rate is slower than 0.02 Vs^{-1}, Figure 5A. At these conditions, the main UPD peak becomes wider too. The main UPD peak is preceded by a smaller shoulder peak centered at ≈ 0.59 V of ΔE. The CV of freshly prepared Ru(0001) surface in 0.1 M $HClO_4$ solution is also shown by red-line in Figure 1. This data indicate that the shoulder peak in cathodic scan of the CV for Pb UPD is related to the onset of Ru-surface oxide/hydroxide reduction[35] (R1 peak). The second reduction peak of the Ru-surface oxide/hydroxide (R2) occurs at lower values of ΔE (0.29 V) and falls into the region between the two UPD peaks (D1 and D2). Therefore, we can conclude that the Pb UPD process is confined within the potential range of the two deposition peaks (D1 and D2) and occurs with preceding and simultaneous Ru oxide/hydroxide reduction process. During anodic sweep, the corresponding Pb UPD ML stripping peaks are observed at 0.225 V (A2) and 0.39 V (A1) of ΔE. The main Pb UPD stripping peak is followed by extended shoulder at 0.45 V ΔE. Its' potential coincides with the onset of the RuOH formation peak (O1-2) indicated in the anodic sweep of the CV for Ru surface in 0.1 M $HClO_4$. The values of Pb UPD stripping peaks are about 0.025 V and 0.07 V more positive than ΔE of corresponding deposition peaks. This suggests an irreversibility of the UPD process. An obvious reason is Ru-surface reduction/oxidation occurring simultaneously with Pb underpotential deposition/stripping. This causes the energetics of the adsorption sites on Ru surface to change between the cathodic and anodic sweeps.[18] The same process is also responsible for ambiguity during the Pb UPD ML charge measurements. Deposition charge of a full ML (q^D_{UPD}) has a quite large values as compared to the Pb UPD ML on other FCC metal surfaces.[3] It equals to 502 ± 16 μC·cm^{-2}. The theoretical charge of the Pb UPD ML with 1x1 structure on Ru(0001) is 512 μC·cm^{-2} ($q^D_{UPD,1x1}$). This value is close to q^D_{UPD} and yet, it is unlikely to be formed on Ru(0001) as it would have a compressive strain values beyond any realistic expectations. Therefore, the origin of such unexpectedly high values for q^D_{UPD} has to be rooted in simultaneous RuOH reduction with Pb UPD process. Earlier studies have shown that formation of the full RuOH ML on Ru(0001) surface equals to a passing charge of approximately 250 μC·cm^{-2}.[31] If this value is subtracted from q^D_{UPD}, the corrected value of the Pb UPD ML deposition charge equals to 252 ± 16 μC·cm^{-2} ($q^D_{UPD,corr}$). This charge corresponds to Pb UPD ML which has about 50% packing density as compared to the hypothetical 1x1 structure. Considering the Pb atom is about 30% bigger than Ru atom,[36] this packing density is realistic scenario and

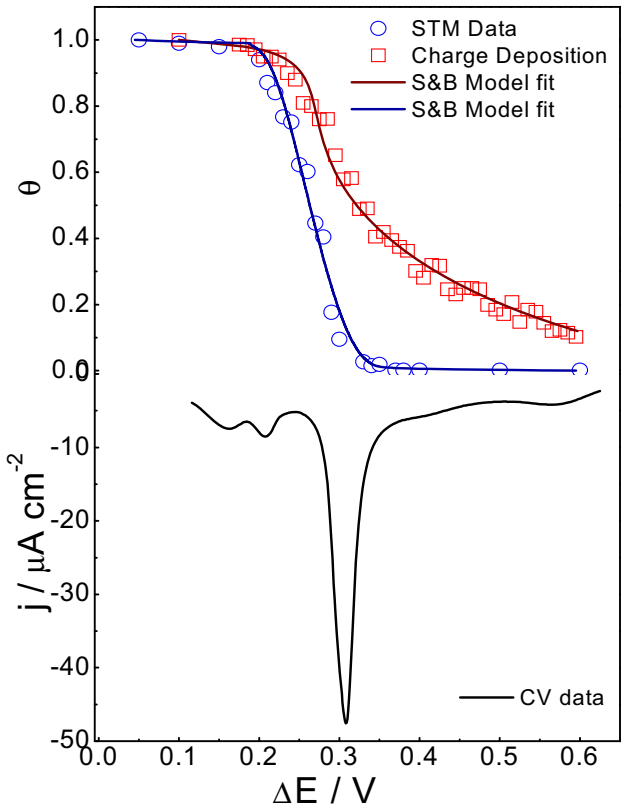

Figure 2. The Pb UPD isotherm data extracted from charge deposition (red-squares) and STM (blue-circle) measurements. The cathodic part of Pb UPD CV is shown for comparison (black). Black line represent the S&B model fit to the data.

is in agreement with Pb ML packing densities reported on other FCC metals with similar atomic diameters.[3]

The isotherm of the Pb UPD on Ru(0001) constructed from charge deposition measurements is presented in Figure 2, red-squares. The simultaneous RuOH reduction with Pb UPD contributes to an isotherm which does not show a classical sigmoidal shape. Additional anomaly is that the coverage of the isotherm does not reach zero at the reference potential of 0.6 V ΔE due to ongoing Ru oxidation process. We notice that isotherms is asymmetric displaying two θ *vs.* ΔE regimes. The first one extents from 0.05 V ÷ 0. 25 V of ΔE and the second one is from 0.25 V ÷ 0.6 V of ΔE. The 0.25 V is the approximate midpoint between those regimes and represents a boundary between the Ru surface free from RuOH (ΔE < 0.25 V), and Ru surface where RuOH is still present (ΔE > 0. 25 V), Figure 1. The extended tale of the isotherm starting from ΔE > 0. 25 V is reflecting the fact that, in parallel with Pb UPD ML formation, a RuOH reduction occurs as well. The solid line in the Figure 2 represents the S&B model fit to the experimental data (Eq. 1). Parameters of the fit are shown in the Table II. We can see that extracted values of the *Frumkin* and *Temkin* parameters are relatively large as compared to other Pb UPD systems/surfaces.[29] In contrary, the value of *m* is much lower than expected. Both discrepancies are likely due to RuOH reduction process occurring in parallel with Pb UPD.

In order to gain mechanistic details of the Pb UPD on Ru(0001), the in situ STM study has been performed. Representative data are shown in Figure 3, images A-J. Detailed analysis of much larger number of STM images than shown in Figure 3 is presented in Figure 2 (STM-isotherm) and Figure 4. Visual inspection of the data in Figure 3 indicate that Ru terraces have presence of small clusters at very positive underpotentials before entering the range of the main UPD peak, 0.36 V < ΔE < 0.5V (Figure 3, image A-C). After processing of these images, we find that in this region of ΔE there is no significant change in cluster density, cluster size (Figure 4) and cluster coverage (Figure 2-blue dots). These clusters gradually lose their contrast as ΔE reaches values closer to the onset of the main UPD peak. Therefore, we attribute their origin to presence of RuOH on the surface. However, entering the region of the main UPD peak, ΔE < 0.36 V, the STM images' morphology starts to change dramatically (Figure 3, images D-E). The cluster density increases drastically which suggests the onset of the nucleation stage (Figure 4B). It reaches the maximum at underpotential which is slightly lower than the main UPD peak (ΔE = 0.29 V). This is also reflected on gradual increase in the Pb ML coverage seen in the Pb UPD isotherm data, Figure 2.

Interestingly, the small plateau in the data shown in Figure 4A indicates that nucleation stage of Pb UPD ML is associated with formation of relatively uniform clusters ($\approx$ 3 nm^2). Further reduction of the underpotential (ΔE < 0.29 V) leads to the growth stage of Pb UPD (images F-J). This is illustrated by gradual decrease in the cluster density due to coalescence and their simultaneous increase in size (Figure 3A) and coverage (Figure 2). Another important result emerges if one has a closer look at images E, F and G. They capture the nucleation and early growth stage of the UPD. They show that local Pb cluster population is noticeably larger at the terrace areas which are in the vicinity of descending steps rather than in the areas near the ascending steps. It appears that Ru steps remain relatively passive for UPD at its early stage. This result is in agreement with RuOH reduction thermodynamics illustrated by CV in Figure 1-red line. The RuOH reduction starts first at terrace sites where thermodynamically less stable RuOH layer exists (R1 peak, Figure 1).[37,38] The steps and other defects on the Ru surface require lower underpotential in order to be freed from RuOH adlayer (R2 peak, Figure 1). Therefore, the thermodynamics of RuOH reduction determines the decoration sequence of the Ru surface by the Pb UPD ML. We can also conclude that decoration of the Ru defects with Pb ML occurs after the main nucleation event already starts on the terraces. This is an interesting peculiarity of this system and similar phenomenon has been observed in the case of Pb UPD on Pt-decorated Au(111) surface.[39]

Within the context of the STM results, we can revisit CV data in Figure 1. It seems that D2 peak at ΔE = 0.2 V does not correlates much with the surface morphology shown in the STM images (Figure 3 vs. Figure 4). Cluster size and coverage data do not seem to be affected significantly in the region of ΔE where this peak is observed. It is clear that the R2 peak, precedes the second Pb UPD peak, D2. In fact, the underpotential where R2 ends is approximately the same as the underpotential where D2 starts. Therefore, the plausible interpretation of the D2 peak is that it corresponds to Pb deposition/decoration at the defect sites which were previously freed from strongly bonded RuOH adlayer. The fact that this peak has potential sweep dependence and disappears with low sweep rates can be attributed to different kinetics of the Pb UPD and RuOH reduction processes. It is likely that

Table II. Extracted parameters of S&B model for Pb UPD and Pb e-less ML.

		Parameters of S&B Isotherm			
Experiment	Data	$\Delta E_{\theta\rightarrow 0}$ / V	*m*	*f*	*g*
UPD-Charge Deposition	Figure 2	0.55 ± 0.03	0.41 ± 0.04	23.5 ± 0.02	−21.0 ± 0.009
UPD - in situ STM	Figure 2	0.31 ± 0.03	2.1 ± 0.005	7.1 ± 0.01	−2.5 ± 0.005
e-less Pb ML dep. - OCP	Figure 5A	0.5 ± 0.02	0.53 ± 0.003	−25.2 ± 0.007	39.0 ± 0.01

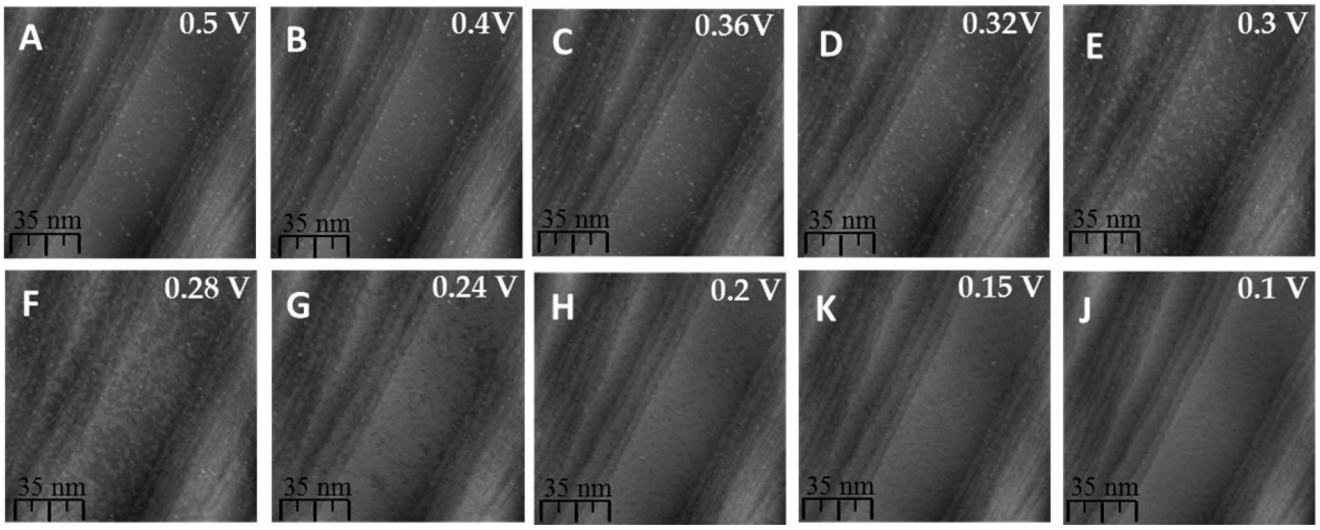

Figure 3. Representative STM images of Ru surface during Pb UPD process. Solution: 0.1M $HClO_4$+10^{-3} M Pb^{2+}. The underpotential at which each image is acquired is indicated at the upper right angle.

Pb UPD is faster than RuOH reduction. At fast sweep rates, separate electrochemical signal from UPD on clean Ru terraces and on steps and defects us due to the slower kinetics of the RuOH reduction which precedes the final stage of the UPD. At slow sweep rates, this is not possible as both processes occur simultaneously and D2 peak disappears. In this case, both processes are convoluted under the one UPD peak as shown in Figure 5A-righ side. Based on the presented discussions we describe each Pb UPD peak in the voltammetry shown in Figure 1 as:

$$\text{D1: } Ru(OH)_{terraces} + Pb^{2+} + 3e^{-} = Pb_{UPD}/Ru_{terraces} + (OH)^{-} \quad [3]$$

$$\text{D2: } Ru(OH)_{defects} + Pb^{2+} + 3e^{-} = Pb_{UPD}/Ru_{defects} + (OH)^{-} \quad [4]$$

In conclusion of the STM data analysis we should point out that the overall shape of the STM-isotherm resembles much better the classical sigmoidal shape. This is not surprising because the STM image segmentation and analysis inherently excludes the complications related to RuOH reduction process. For this reason, the corresponding S&B isotherm model (solid line) yields parameters with more realistic values, Table II.[29]

Electroless (e-less) Pb monolayer deposition on Ru(0001).— Following the experimental routine for the e-less Pb ML deposition described previously, the OCP transient of Ru(0001) is recorded during addition of V^{2+} containing aliquot into 0. 1 M $HClO_4$ + 10^{-3} M Pb^{2+} solution. Data are presented in Figure 5A-left side. It is noticeable that upon addition of V^{2+} (t = 68 sec), the OCP starts to change abruptly and drifts towards more negative values. Approximately after additional 60 seconds, the OCP transient enters a steady state, $E^{S}_{OCP} \approx -0.450$ V vs. Ag/AgCl. The solid line in the Figure 5A represents the model fit (Eq. 2) to the OCP transient. The parameters of the S&B isotherm extracted from the fit are presented in Table II.

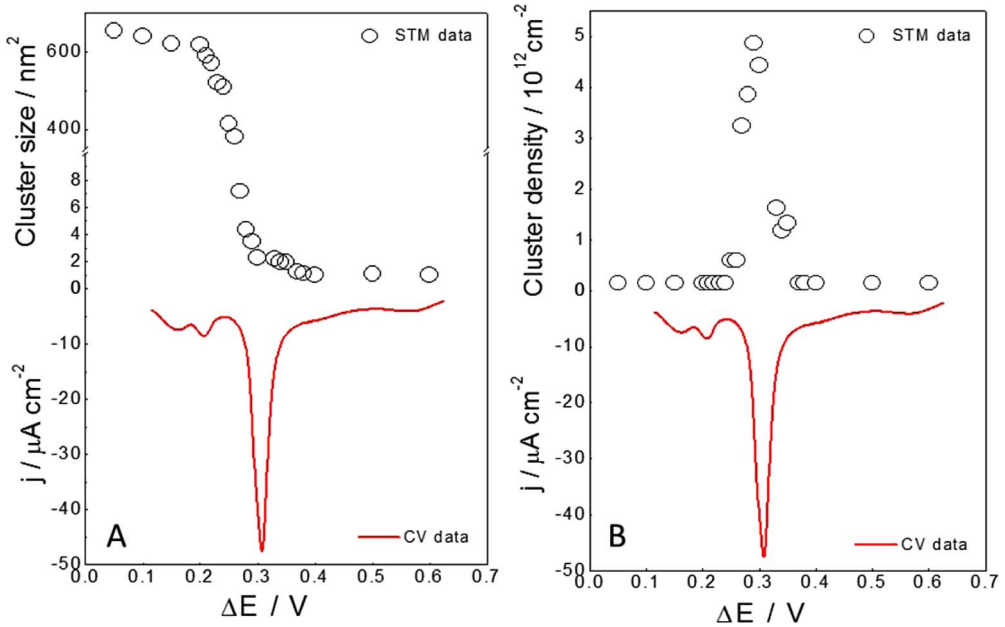

Figure 4. Combined STM analysis and electrochemical results for Pb UPD on Ru(0001). (A) Cluster size vs. ΔE and (B) Cluster density vs. ΔE. The cathodic sweep of the CV in Figure 1 is presented at lower part of each graph.

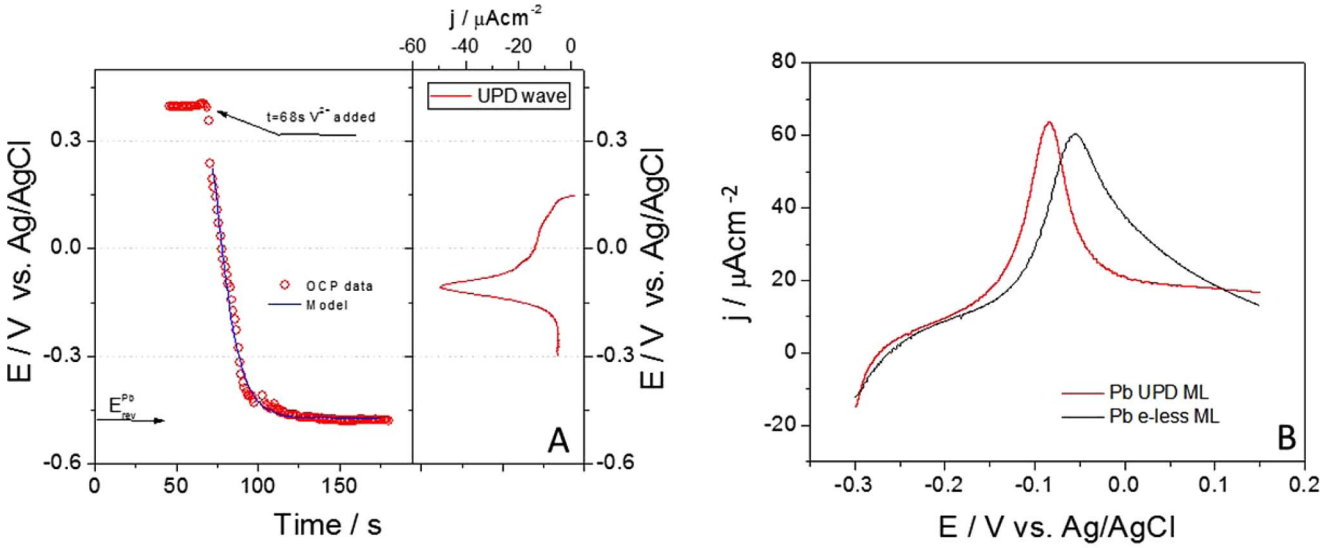

Figure 5. (A) OCP transient during the e-less Pb ML deposition on Ru(0001) – left side, and cathodic sweep of Pb UPD CV (dE/dt= 0.01 Vs^{-1}) recorded prior to execution of the e-less procedure – right side. Solution formulation presented in Table I. (B) Stripping wave for the e-less Pb ML in 0.1 M $HClO_4$ solution (black) and UPD Pb ML (red) in $HClO_4 + 10^{-3}$ M Pb^{2+} solution, dE/dt = 0.01 Vs^{-1}.

It should be emphasized that the value of E^S_{OCP} is just few millivolts more positive than the Pb reversible potential marked in Figure 5A as well. For comparison, on the right side of the same figure, the cathodic wave from the CV of Pb UPD on Ru(0001) recorded prior to the addition of V^{2+} aliquot is plotted having a common potential axes. One can see that the value of the OCP drifts though the entire region of the Pb UPD. Obviously, the value of E^S_{OCP} resides at potentials where the full Pb UPD ML is stable. Therefore, we expect that Pb ML should be stable on Ru(0001) at OCP conditions in solution which contains both, V^{2+} and Pb^{2+} ions. To verify this, and prove that actual deposition of Pb has happened, the Ru crystal is immediately transferred into 0.1 M $HClO_4$ solution and anodic sweep is performed having the same starting potential as the negative sweep limit of the previously recorded CV (−0.3 V vs. Ag/AgCl). The stripping wave is shown in Figure 5B – black line. It is evident that its shape is similar to the one of the full Pb UPD ML (red line). However, the unexpected result is that the e-less Pb ML stripping peak potential is about 0.05 V more positive than the one for Pb UPD ML. This observation is even more surprising knowing that the stripping of the e-less Pb ML was done in solution which does not contain Pb^{2+} ions. More positive stripping potential suggests that the e-less Pb ML is more stable than corresponding Pb UPD ML. Yet, for conditions at which the e-less Pb ML stripping is performed, an opposite result is expected.[19] An additional result is that about 10% more charge is associated with the e-less Pb ML stripping than in the case of Pb UPD ML ($q^S_{e-less} = 550 \pm 7$ μC·cm^{-2} and $q^S_{UPD} = 505 \pm 11$ μC·cm^{-2}). We have investigated this issue further and performed comparative ECQMB measurements for the Pb UPD and e-less Pb ML deposition using the same Ru/quartz crystal. These data are shown in Figure 6.

ECQMB results shown that frequency change during the e-less Pb ML deposition is about 20% larger than for the Pb UPD i.e. about 20% larger mass is associated with formation of the e-less Pb ML (Figure 6). This finding is in qualitative agreement with larger charge recorded during the e-less Pb ML stripping. Indeed, the stripping charge

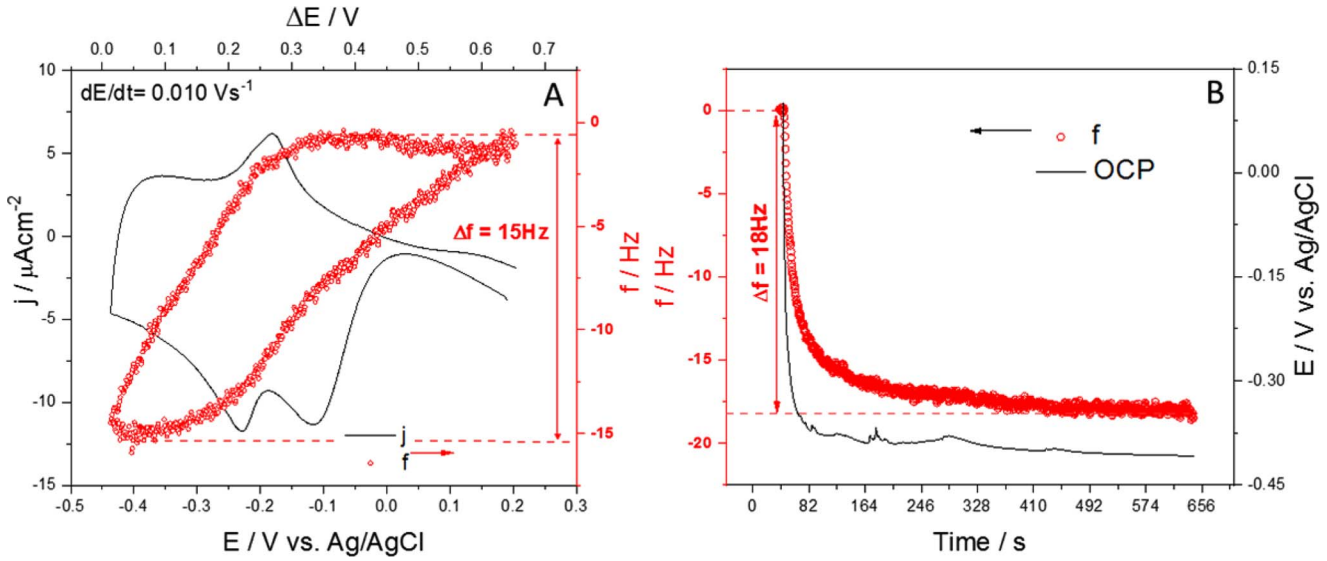

Figure 6. (A) ECQMB and CV data for Pb UPD ML deposition/stripping, solution: $HClO_4 + 10^{-3}$ M Pb^{2+}. (B) ECQMB data and OCP transient during e-less Pb ML deposition. Solution description in Table I.

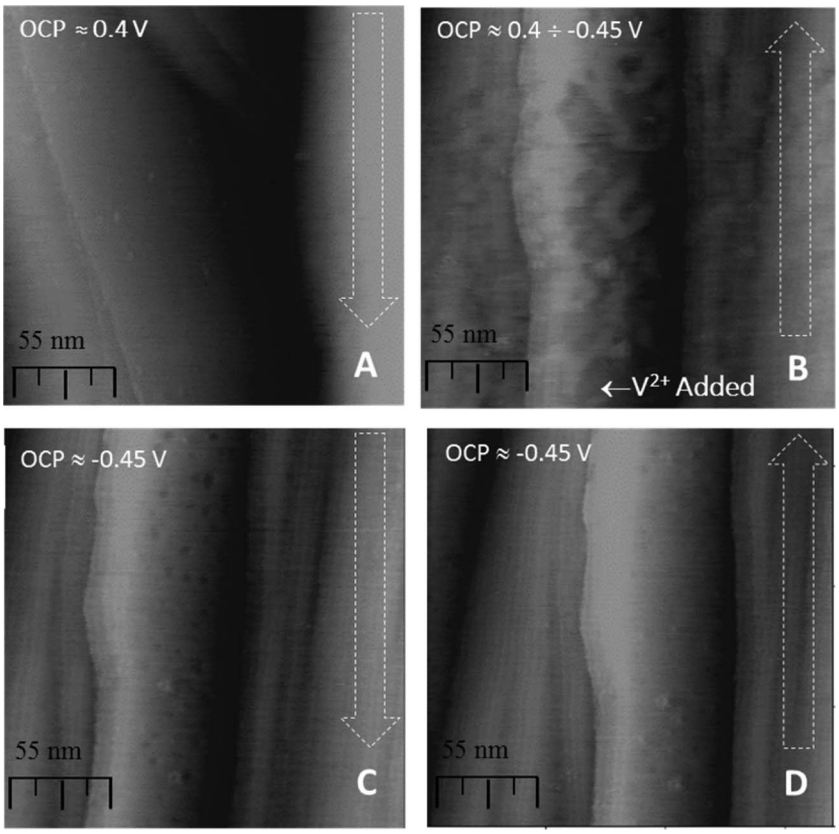

Figure 7. In situ STM images of Ru surface during e-less Pb ML deposition process. The value of OCP at which each image is acquired is indicated at the upper left angle. Scan direction is indicated by an arrow.

difference between the e-less Pb ML and Pb UPD ML is about 50 $\mu C \cdot cm^{-2}$ which represents about 20% of the charge calculated for the full Pb UPD ML deposition ($q^{D}_{UPD,corr} = 252 \pm 16\ \mu C \cdot cm^{-2}$). Obviously, both measurements suggest formation of an e-less Pb ML which has about 20% more mass/charge than what is calculated for the full Pb UPD ML. One explanation is that e-less Pb ML could have a structure which has about 20% higher packing density than the Pb UPD ML. Perhaps, if real, this structure would be associated with a significant compressive strain and formation of *Morrie* patterns in the Pb layer. It has to be mentioned that other explanation may include a formation of a limited amount of 3D Pb phase during e-less deposition process. At the same time, as a counter argument, one should keep in mind that E^{S}_{OCP} resides in an underpotential region where the 3D Pb phase is thermodynamically unstable/dissolved.

To gain more information about the e-less Pb ML deposition, we have performed an in situ STM study. Results are presented in Figure 7. Image A shows a clean Ru(0001) surface in solution with 10^{-3}M Pb^{2+} + 0.1M $HClO_4$ at open circuit (≈ 0.4V vs. Ag/AgCl). Many features of a single crystal Ru surface such as steps and terraces are evident. A few clusters of monoatomic height are also visible on Ru terraces. At the beginning of the image B, the V^{2+} containing aliquot is added to the STM cell. The moment of addition is indicated by an arrow. During acquisition of the remaining part of the image B, the OCP drifts though the potential region where Pb UPD ML deposition occurs (0.4 V – −0.45 V). Consequently, the morphological changes on the Ru surface are associated with formation of the Pb ML. Considering that STM image acquisition is relatively slow process (200 sec per image) the image B shows a convolution of nucleation and growth processes from the moment of V^{2+} addition. At the beginning of the image B, the Ru surface is just partially covered by Pb clusters which evolve into almost complete ML by the end the scan. It is noticeable that the e-less Pb ML growth occurs at terraces starting from regions closer to descending steps. This spatial bias in the growth dynamics on Ru terraces has been already observed and discussed during the Pb UPD (image E-G in Figure 4). Apparently, the passivity of the Ru steps due to strongly bonded RuOH also affects the decoration sequence of Ru surface by the e-less Pb ML. Further on, in image C, one can see a gradual smoothening of the surface and the emergence of a continuous 2D layer morphology i.e., a full e-less Pb ML. At the same time, the OCP reaches its steady state, $E^{S}_{OCP} \approx -0.45$ V. As a final stage, in image D, the morphology of complete Pb ML is evident with no indication of 3D growth. One can recognize a great similarity between the e-less Pb ML and the Pb UPD ML by comparison of image D in Figure 7 and image J in Figure 3. We can conclude that the in situ STM results in Figure 7 are in agreement with conclusion derived from the OCP transient, $E^{S}_{OCP} > E^{rev}_{Pb}$ (Figure 5A), i.e. there is no 3D Pb phase formation during the e-less Pb ML deposition process. However, we have to note that in situ STM could not resolve any *Morrie* pattern or other higher order structure on either Pb ML (Figure 3 and Figure 7). This leaves us with the puzzle about the similarity between the morphologies of the Pb UPD ML and the e-less Pb ML which seems to contradict their difference in stripping charge and mass change measurements.

Perhaps more answers and insight in the mutual difference and similarity between the Pb UPD ML and the e-less Pb ML is at our grasp if we consider data in Table II.

As one can see, the S&B parameters obtained from fitting electrochemical data (Figure 2 and Figure 5A) are in good mutual agreement in terms of their magnitudes. The values of *m* are close for both deposition processes. The *m* being < 2, is unrealistic results if one considers the charge of the Pb ion. However, knowing that, in parallel with Pb^{2+} ML deposition, a RuOH reduction occurs as well, the result is not surprising. The same discussion does apply to the values of $\Delta E_{\theta \to 0}$ parameter. The S&B isotherm fits of the electrochemical data for both deposition processes yield significantly more positive values than what is obtained from fits of the STM data. The RuOH reduction precedes the Pb ML deposition process, therefore, the extracted values of $\Delta E_{\theta \to 0}$ likely contain the information about the underpotential where RuOH reduction starts rather than about onset of either Pb ML deposition. Based on these arguments, it is reasonable to assume that the e-less Pb ML deposition process involves the same processes on Ru surface as in the case of the UPD. Therefore, its description can

be written as:

$$Ru(OH) + Pb^{2+} + 3V^{2+} = Pb_{e-less}/Ru + 3V^{3+} + (OH)^{-} \quad [5]$$

The framework of S&B isotherm analysis yields important information about the interactions associated with the e-less and UPD Pb ML. The magnitudes of f and g interaction parameters obtained from the electrochemical data are similar yet with opposite signs. They are also almost an order of magnitude larger than the ones extracted from the STM data. Their opposite signs mean that the predominant nature of interaction between Ru substrate and the e-less Pb ML is repulsive while it is attractive in the case of the Pb UPD ML. On the other hand, the interactions among the adatoms with in the e-less Pb ML express attractive forces while UPD adatoms show repulsive. No doubt, the data in Table II point to an apparent paradox existing between two Pb ML with very similar morphologies produced by two different process. One way that we can explain this is by revoking a "third body" or anion co-adsorption phenomenon. Namely, it is possible that some portion of the V^{2+} ions adsorbed on the RuOH or clean Ru surface are trapped by Pb ML during deposition process. It is likely that they are trapped at the interface between Ru and Pb or in-between Pb adatoms within the ML. The possibility that they could be co-adsorbed on the top of the Pb ML cannot be excluded too. The charge of V^{2+} and its reducing power can mitigate the nature of the interactions in the e-less Pb ML resulting that the f and g parameters have sign inversion as compared to the Pb UPD ML. The proposed hypothesis explains easily the higher stability of the e-less Pb ML and the extra charge and mass associated with the e-less Pb ML depostion/stripping. However, at this point we have to admit that more experiments are necessary to fully confirm these arguments or perhaps provide a more complete description of the e-less Pb ML structure.

Conclusions

Two different ways of Pb ML deposition on Ru(0001) were demonstrated using UPD and e-less deposition phenomenon. In each approach, a 2D deposit is obtained with very similar morphology. The electrochemical data suggest that the Pb ML deposition process is affected by the kinetics and thermodynamics of RuOH reduction. This reflects on the decoration sequence of the Ru surface by Pb ML where the nucleation and growth is first observed on terraces rather than on surface steps and defects. The same phenomenon is responsible for atypical shape of the Pb ML adsorption isotherm and on corresponding parameters of the S&B model. The difference between e-less Pb ML and Pb UPD ML is demonstrated in the mass/charge associated with their formation and stripping. This also reflected on the opposite signs of corresponding interaction parameters between the e-less and UPD Pb ML. At present, these results could have different interpretations and more studies are necessary to discern their true origin. It is certain that this study should serve as a prelude in development other Pb ML assisted epitaxial growth protocols on Ru surface or implementation of thin film growth methods which utilize Pb ML as a reducing agent in SLRR reaction.

Acknowledgment

The experimental material is based upon work supported in part by the National Science Foundation under the contract CBET 1605331 and Lam Research Corporation gift grant.

ORCID

S. R. Brankovic https://orcid.org/0000-0001-8250-8382

References

1. S. Trasatti, *J. Electroanal. Chem.*, **33**, 351 (1971), see Ref. therein.
2. D. M. Kolb, *in Advances in Electrochemical Eng*., H. Gerischer and W. Tobias, Editors, Wiley & Sons, New York (1978), see Ref. therein.
3. E. Budevski, G. Staikov, and W. J. Lorenz, in *Electrochemical Phase Formation and Growth*, R. C. Alkire, H. Gerischer, D. M. Kolb, and C. W. Tobias, Editors, p. 41, VCH, Berlin (1996). and Ref. therein.
4. E. Herrero, L. J. Buller, and H. D. Abruña, *Chem. Rev.*, **101**, 1897 (2001).
5. K. Sieradzki, S. R. Brankovic, and N. Dimitrov, *Science*, **284**, 138 (1999).
6. S. R. Brankovic, N. Dimitrov, and K. Sieradzki, *Electrochem. Solid State Lett.*, **2**, 443 (1999).
7. J. Lipkowski and P. N. Ross, *Electrocatalysis*, p. 59 and p. 225., Wiley-VCH, New York (1998).
8. M. B. Vukmirovic, N. Dimitrov, and K. Sieradzki, *J. Electrochem. Soc.*, **149**, B428 (2002).
9. Y. Liu, S. Bliznakov, and N. Dimitrov, *J. Phys. Chem. C*, **113**, 12362 (2009).
10. M. Fayette, Y. Liu, D. Bertrand, J. Nutariya, N. Vasiljevic, and N. Dimitrov, *Langmuir*, **27**, 5650 (2011).
11. L. T. Viyannalage, R. Vasilic, and N. Dimitrov, *J. Phys. Chem. C*, **111**, 4036 (2007).
12. S. R. Brankovic, J. X. Wang, and R. R. Adzic, *Surf. Sci.*, **474**, L173 (2001).
13. N. Dimitrov, *Electrochim. Acta*, **209**, 599 (2016).
14. S. R. Brankovic, N. Vasiljevic, and N. Dimitrov, in *Chapter 27- Applications to Magnetic Recording and Microelectronic Technologies*, Modern Electroplating V, M. Paunovic and M. Schlesinger, Editors, p. 573, John Willey and Sons, Inc (2010).
15. R. Vasilic, L. T. Viyannalage, and N. Dimitrov, *J. Electrochem. Soc.*, **153**, C648 (2006).
16. Y. G. Kim, J. Y. Kim, D. Vairavapandian, and J. L. Stickney, *J. Phys. Chem. B*, **110**, 17998 (2006).
17. S. Ambrozik, B. Rawlings, N. Vasiljevic, and N. Dimitrov, Metal Deposition via Electroless Surface Limited Redox Replacement. *Electrochem. Commun.*, **44**, 19 (2014).
18. D. Wu, D. J. Solanki, A. Joi, Y. Dordi, N. Dole, D. Litvinov, and S. R. Brankovic, *J. Electrochem. Soc.*, **166**, D3013 (2019).
19. D. Wu, D. J. Solanki, J. L. Ramirez, W. Yang, A. Joi, Y. Dordi, N. Dole, and S. R. Brankovic, *Langmuir*, **34**, 11384 (2018).
20. K. Venkatraman, A. Joi, Y. Dordi, and R. Akolkar, *Electrochemistry Comm*., **91**, 45 (2018).
21. M. Will, M. Dietterle, and D. Kolb, in *Nanoscale Probes of the Solid/ Liquid Interface*, vol **288**, A. Gewirth and H. Siegenthaler, Editors, p. 137, Springer, Berlin (1995).
22. S. Garcia, D. Salinas, and G. Staikov, *Surf. Sci.*, **576**, 9 (2005).
23. S. Corcoran, G. Chakarova, and K. Sieradzki, *J. Electranal Chem.*, **377**, 85 (1994).
24. M. Esplandiu, M. Schneeweiss, and D. Kolb, *Phys. Chem. Chem. Phys.*, **1**, 4847 (1999).
25. K. Engelsmann, W. Lorenz, and E. Schmidt, *J. Electroanal. Chem.*, **114**, 1 (1980).
26. E. Schmidt, H. Gygax, and P. Bohlen, *Helv. Chim. Acta*, **49**, 733 (1966).
27. R. Adzic, E. Yeager, and B. Cahan, *J. Electrochem. Soc.*, **121**, 474 (1974).
28. A. Bewick and B. Tomas, *J. Electroanal. Chem.*, **84**, 127 (1977).
29. S. Swathirajan and S. Burckenstein, *Electrochim. Acta*, **28**, 865 (1983).
30. S. R. Brankovic, J. X. Wang, and R. R. Adzic, *Electrochem. Solid State Lett.*, **4**, A217 (2001).
31. S. R. Brankovic, J. X. Wang, Y. Zhu, R. Sabatini, J. McBreen, and R. R. Adzic, *J. Electroanalytical. Chemistry*, **231**, 524, (2002).
32. D. Gokcen, *Morphology and Property Control of Pt Submonolayers Deposited via Surface Limiter Redox Replacement Reaction*, Ph.D. Thesis, University of Houston (2010).
33. N. Otsu, *IEEE Transactions on Systems, Man and Cybernetics IEEE T.*, Syst. Man Cyb., SMC-9, **62**, (1979).
34. D. Gokcen, S. E. Bae, and S. R. Brankovic, *J. Electrochem. Soc.*, **157**, D582 (2010).
35. S. R. Brankovic, J. X. Wang, Y. Zhu, R. Sabatini, J. McBreen, and R. R. Adzic, *J. Electroanal. alChem.*, **231**, 524 (2002).
36. B. D. Cullity and S. R. Stock, *Elements of X-Ray Diffraction*, p. 624, Prentice Hall, NJ (2001).
37. W. F. Lin, M. S. Zei, Y. D. Kim, H. Over, and G. Ertl, *J. Phys. Chem. B*, **104**, 6040 (2000).
38. M. B. Vukmirovi, R. L. Sabatini, and R. R. Adzic, *Surf. Sci.*, **572**, 269 (2004).
39. Q. Yuan, A. Tripathi, M. Slavkovic, and S. R. Brankovic, *Z. Phys. Chem.*, **226**, 965 (2012).